DESIGN AND SIMULATION OF A TRIPLE ABSORBER LAYER PEROVSKITE SOLAR CELL FOR HIGH CONVERSION EFFICIENCY

Abderrahim Yousfi[a]*, Okba Saidani[a], Zitouni Messai[a], Rafik Zouache[b]
Mohamed Meddah[a], Younes Belgoumri[a]

[a] *ETA Laboratory, Department of electronics, Faculty of technology, University Mohamed El Bachir El Ibrahimi of Bordj Bou Arréridj-34030, Algeria*
[b] *Electronic Department, Faculty of Technology, University of Msila, 28000, Algeria*
***Corresponding Author e-mail: Abderrahim.yousfi@univ-bba.dz**

This paper presents a comprehensive simulation study on the influence of a triple absorber layer configuration in a perovskite-based solar cell using the SCAPS-1D software, under AM1.5 illumination. The simulated structure comprises a Cesium Tin-Germanium Triiodide ($CsSn_{0.5}Ge_{0.5}I3$) absorber layer sandwiched between Indium gallium zinc oxide (IGZO) and Cu_2O layers. The main objective of this study is to enhance the power conversion efficiency (PCE) by optimizing the thicknesses of each layer. To validate our simulation results, we compare them with experimental data obtained from existing literature, and we observe a satisfactory agreement between the two. Our findings reveal that the maximum PCE of 28% can be achieved by utilizing specific thickness values for each layer. Specifically, the optimal thicknesses are determined to be 20 nm for the IGZO layer, 200 nm for the Cu_2O layer, and 700 nm for the perovskite layer. These optimized thickness values lead to a significant improvement in the PCE of the solar cell, reaching 29%. This achievement highlights the effectiveness of our proposed triple absorber layer configuration and demonstrates its potential to enhance the overall performance of the perovskite-based solar cell. Overall, this study provides valuable insights into the optimization of the absorber layer configuration in perovskite solar cells, leading to improved power conversion efficiency.

Keywords: *Perovskite solar cell, $CsSn_{0.5}Ge_{0.5}I3$; Power conversion efficiency; SCAPS-1D*
PACS: 84.60.Jt

1. INTRODUCTION

Hybrid perovskite materials have gained significant attention in the field of solar cells due to their remarkable properties and their potential as a low-cost solution for photovoltaic applications [1-10]. These materials have experienced a rapid increase in photovoltaic conversion efficiency, rising from approximately 3.9% in 2009 to 25.2% in 2021 [11-14]. Their exceptional characteristics, such as tunable bandgap, long diffusion length, efficient carrier transport, and ease of fabrication, have positioned them as strong competitors to traditional silicon-based solar cells. However, the commercial development of lead halide perovskites is hindered by the issue of lead toxicity. To address this challenge, researchers have been exploring alternative materials with lower toxicity, and among them, tin-based (Sn-based) perovskites have demonstrated promising results, particularly with Sn_2^+ showing the highest power conversion efficiency. Different studies have investigated Sn-based perovskites, including FASnI3, MASnI3, and CsSnI3, revealing that organo-based perovskites inherently exhibit low stability. This has led to Cs-based cation perovskite, specifically CsSnI3, emerging as the preferred candidate [15]. In the search for lead-free alternatives, planar heterojunction architecture has been explored as a viable option for Sn-based perovskites. However, Sn-based devices face challenges related to rapid oxidation of Sn_2^+ to Sn_4^+ when exposed to air, resulting in device instability and degradation. Furthermore, the self-doping of p-type materials increases the concentration of holes, leading to enhanced carrier recombination rates, which is detrimental to cell performance [16-20]. To overcome these issues, researchers have proposed alloying CsSnI3 with Ge_2^+ to create CsSn0.5Ge0.5I3 perovskite configuration, which exhibits improved stability and air tolerance [21]. This configuration possesses favorable structural stability factors, including a Goldschmidt tolerance factor of 0.94 and an Octahedral factor of 0.4, contributing to the overall stability of the perovskite solar cell. Additionally, the addition of SnF2 to Sn-based perovskites has been shown to effectively reduce the oxidation of Sn_2^+ to Sn_4^+, resulting in enhanced stability [22-24]. Devices fabricated with SnF2 have demonstrated performance stability for extended periods, maintaining 98% of their initial power conversion efficiency for over 100 days. Despite advancements in improving the performance of Sn-based perovskite solar cells, their power conversion efficiency still remains relatively low. Therefore, it is crucial to gain a comprehensive understanding of the relationship between material parameters and device architecture to enhance the performance of $CsSn_{0.5}Ge_{0.5}I3$-based devices. In this work, we report on the design and simulation of a novel IGZO / $CsSn_{0.5}Ge_{0.5}I3$ / CsSnCI3 / CsSnCI3 / Cu_2O / Spiro-OMeTAD solar cell configuration using SCAPS-1D software [37]. The objective is to investigate the impact of a triple absorber layer configuration and varying thicknesses on key performance parameters such as short-circuit current density (Jsc), open circuit voltage (V_{OC}), fill factor (FF), and overall power conversion efficiency (PCE). The obtained results offer valuable insights for the design and development of high-performance $CsSn_{0.5}Ge_{0.5}I3$ perovskite solar cells.

2. DEVICE SETTINGS AND SIMULATION PROCESS

The device structure used in the simulations is based on the numerical design mentioned in reference [25]. It consists of the following layers: IGZO / CsSn0.5Ge0.5I3 / CsSnCI3 / CsSnCI3 / Cu$_2$O / Spiro-OMeTAD, as illustrated in Figure 1. In this structure, IGZO with a thickness of 0.015 μm serves as the electron transport material (ETL). IGZO is chosen for its favorable band alignment, excellent optoelectronic properties, and stability [26,27]. Cu$_2$O [28], with a thickness of 0.4 μm, is used as the hole transport layer (HTL), which is commonly employed in high-efficiency solar cells. The n-type absorber layer consists of a mixed halide perovskite (CsSn0.5Ge0.5I3, CsSnCl3, CsSnCl3) with a thickness of 0.250 μm. In this structure, the HTL and ETL layers are n-type and p-type, respectively. Various parameters were employed for the simulation of each layer, as summarized in Table 1. The input parameters for IGZO, Spiro OMeTAD, and CsSn$_{0.5}$Ge$_{0.5}$I3 were adopted from a similar simulation structure documented in the literature [29-31]. The absorption coefficients for the absorber and HTL were obtained from relevant literature sources [35-36]. Additionally, the SCAPS-1D software library, specifically the SOPRA database, provided the required absorption coefficients for the ETL layer. The band gap equation for the mixed halide perovskite CsSn$_{0.5}$Ge$_{0.5}$I3, expressed as a function of x, was derived from a numerical reference [22]. Moreover, the simulations were conducted at an operating temperature of 300 K. By utilizing this simulated device structure and incorporating the appropriate parameters and equations, the study aims to gain insights into the performance characteristics of the perovskite solar cell under investigation.
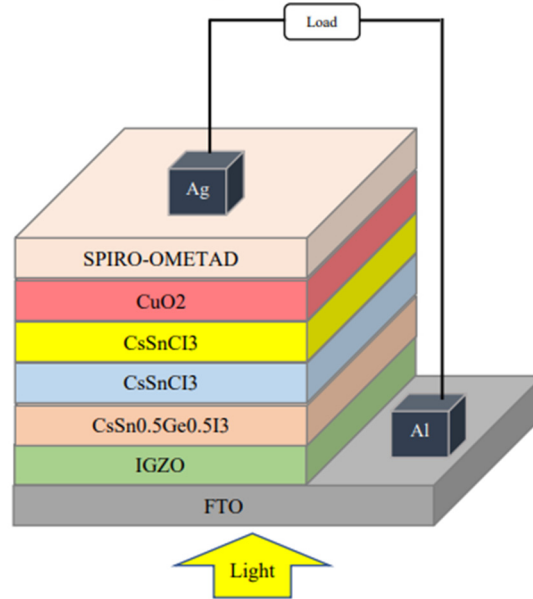
Figure 1. Structure of the suggested solar cell-based perovskite.

SCAPS-1D, also known as Solar Cell Capacitance Simulator One Dimension, is a software application designed for Windows. It was developed at the University of Gent using lab windows/CVI of the national instrument. The primary purpose of this program is to numerically solve fundamental semiconductor equations in a one-dimensional context, specifically under steady-state conditions. By utilizing SCAPS-1D, users are able to define various parameters upon which the program calculates results. These results provide valuable insights into the underlying physics of the model, offering explanations for important aspects such as individual carrier densities, carrier transport mechanisms, electric field distributions, and recombination profiles., which are given below [38]:

$$\left(\frac{\partial^2 \psi}{\partial x^2}\right) = -\frac{\partial E}{\partial x} = -\frac{\rho}{\varepsilon_s} = -\frac{q}{\varepsilon_s}\left[p - n + N_d^+ - N_a^- + N_{def}\right]. \tag{1}$$

Where Ψ is electrostatic potentiality, εs is static relative permittivity, q is the charge, e and n are the respective electrons and holes, $Nd+$ is density of donor, $N\alpha-$is density of acceptor and $Ndef$ is the defect density of both donor and acceptor. The carrier continuity equation in device may be represented as given below:

$$-\frac{\partial j_p}{\partial x} + G - U_p(n,p) = 0, \tag{2}$$

$$-\frac{\partial j_n}{\partial x} + G - U_n(n,p) = 0. \tag{3}$$

Here j$_p$ and j$_n$ are the hole and electron current densities, G is carrier generation rate, U$_n$ (n, p) and U$_p$ (n, P) are the recombination rates of electrons and holes respectively. Furthermore, carrier current density may also be obtained from:

$$j_p = qn\mu_p E + qD_p \frac{\partial n}{\partial x}, \tag{4}$$

$$j_n = qn\mu_n E + qD_n \frac{\partial n}{\partial x}.$$ (5)

Here q is the charge, μp and μn are carrier mobilities, and D_p, D_n are the diffusion coefficients.

By conducting simulations using SCAPS-1D [32-33], it is possible to obtain values for current density (Jsc), power conversion efficiency (PCE) as a percentage, fill factor (FF) as a percentage, and open circuit voltage (Voc) for different thicknesses and temperatures. These simulations are applicable to seven distinct layers of the solar cell and can be performed under both illuminated and dark conditions, considering a range of temperatures [37].

3. RESULTS AND DISCUSSION

To enable an efficient extraction of electrons and holes from the perovskite active layer in photovoltaic devices, certain requirements must be met. Specifically, the electron affinity (EA) of the electron transport layer (ETL) should be greater than that of the perovskite, while the hole transport layer (HTL) should have a lower EA than the perovskite [34]. This ensures favorable energy level alignment for the extraction of charge carriers. In our simulated device components, these conditions have been successfully fulfilled, as demonstrated in Table I. Additionally, for proper electron flow from the perovskite to the ETL, the conduction band of the ETL should be situated lower than that of the perovskite. Conversely, to prevent the undesirable backflow of electrons in the opposite direction, the conduction band of the HTL should be higher than that of the perovskite. These considerations ensure unidirectional charge transport. Likewise, to facilitate the flow of holes from the perovskite to the HTL, the valence band of the HTL should be positioned higher than that of the perovskite. Conversely, the valence band of the ETL should be lower than that of the perovskite to prevent the backward movement of holes. By satisfying these band alignment requirements, we ensure the efficient extraction and separation of electrons and holes within the device.

Table 1. Properties of the different layers of the proposed structure.

Parameters	IGZO	CsSn0.5Ge0.5I3	CsSnCl3	CsSnCl3	CuO2	Spiro-OMeTAD
Thickness (um)	0.015	0.250	1.000	1.000	0.400	0.100
Band gap (eV)	3.050	1.498	1.220	1.220	3.700	4.005
Electron affinity (eV)	4.160	4.000	3.800	3.700	1.700	1. 460
Dielectric Permittivity	10.00	28.000	20.000	20.000	10.000	10.700
CB effective density of states (cm^{-3})	5.000E+21	3.100E+18	5.000E+16	5.000E+16	2.200E+19	2.800E+20
VB effective density of states (cm^{-3})	5.000E+16	3.100E+19	5.000E+16	5.000E+16	1.800E+18	1.000E+20
19 Electron mobility (cm^2/VS)	1.500E+1	9.740E+2	5.000E+1	7.000E+1	1.000E+2	1.200E+1
Hole mobility (cm^2/VS)	1.000E-1	2.130E+2	5.000E+1	5.000E+1	2.500E+1	2.800E+0
Shallow uniform donor density N_D (cm^{-3})	1.000E+18	0.000E+0	0	0	0	0
Shallow uniform acceptor density N_A (cm^{-3})	1.000E+5	1.100E+18	1.000E+20	1.000E+210	2.000E+21	1.000E+21

The fulfillment of these crucial conditions is illustrated in Figure 2, providing visual evidence of the desired energy level alignment and band structures necessary for effective charge carrier extraction and transport in the perovskite-based photovoltaic device.

To comprehensively assess the behavior and performance of the IGZO / CsSn$_{0.5}$Ge$_{0.5}$I3 / CsSnCI3 / CsSnCI3 / Cu$_2$O / Spiro-OMeTAD solar cell, we conducted a series of simulations. Our objective was to investigate the impacts of the Triple Absorber Layer Perovskite and the thicknesses of the electron transport layer (ETL) and the hole transport layer (HTL) on the efficiency of perovskite-based solar cells.
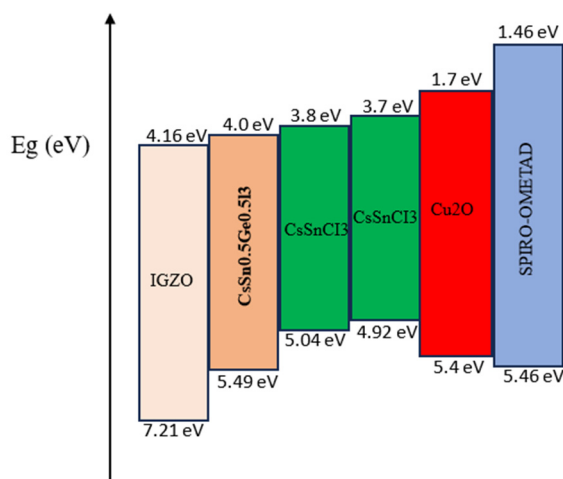
Figure 2. Energy band diagram of the materials used in the simulation. The units for the band energies are in electron volt (eV)

3.1. Effect of the first perovskite layer (CsSn$_{0.5}$Ge$_{0.5}$I3) thickness:

In this section, we aim to investigate the performance of the IGZO / CsSn$_{0.5}$Ge$_{0.5}$I3 / CsSnCI3 / CsSnCI3 / Cu$_2$O / Spiro-OMeTAD solar cell using the parameters provided in Table 1. Our focus is on determining the optimal thickness of the CsSn$_{0.5}$Ge$_{0.5}$I3 absorber layer. Figure 3 presents the evolution patterns of key parameters, including open-circuit voltage (Voc) (Figure 3(b)), short-circuit current density (Jsc) (Figure 3(a)), fill factor (FF) (Figure 3(c)), and overall power conversion efficiency (PCE) (Figure 3(d)), as a function of the n-CsSn0.5Ge0.5I3 absorber layer thickness ranging from 0.2 to 0.65 μm. With an increase in the thickness of the CsSn$_{0.5}$Ge$_{0.5}$I3 layer from 0.25 to 0.65 μm, a significant enhancement in Jsc is observed, rising from 38.4 mA/cm^2 to approximately 38.43 mA/cm^2. This rise in Jsc can be attributed to the increased path length for photon absorption, resulting in the generation of a higher number of charge carriers. Additionally, the fill factor (FF) displays a remarkable increase from 56.5% to approximately 66.5% as the CsSn$_{0.5}$Ge$_{0.5}$I3 layer thickness increases. The higher FF indicates improved charge extraction and reduced losses within the solar cell, contributing to enhanced overall performance. Conversely, there is a decrease in the open-circuit voltage (Voc) as the absorber layer thickness increases. Voc decreases from 1.35 V to approximately 1.05 V. At a thickness of 0.25 μm, a higher Voc is observed, indicating reduced recombination. However, as the absorber thickness increases, the generation of more carriers leads to an enhancement in recombination, causing a decline in Voc. The observed variations in Voc, Jsc, and FF have direct implications for the overall power conversion efficiency (PCE) of the solar cell. Optimal thickness selection must strike a balance between maximizing Jsc and FF while minimizing the loss in Voc due to increased carrier generation and recombination. It is worth noting that these findings highlight the influence of the CsSn$_{0.5}$Ge$_{0.5}$I3 absorber layer thickness on the performance parameters of the solar cell. Careful consideration of these variations is crucial in optimizing the device's PCE.
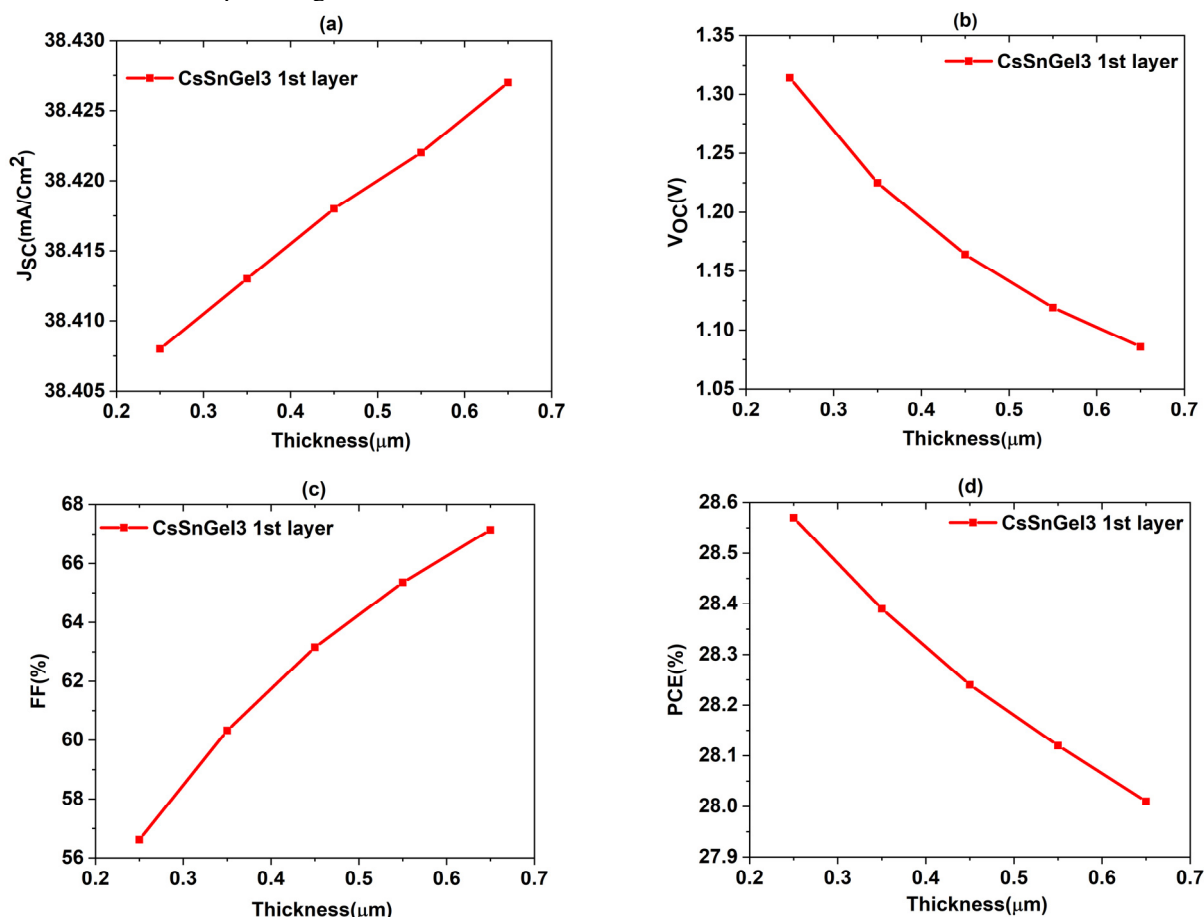
Figure 3. Effect of the first perovskite layer (CsSn0.5Ge0.5I3) thickness

3.2. Effect of the second perovskite layer (CsSnCI3) thickness:

The effect of the n-CsSnCI3 absorber layer thickness on the performance of the IGZO / CsSn$_{0.5}$Ge$_{0.5}$I3 / CsSnCI3 / CsSnCI3 / Cu$_2$O / Spiro-OMeTAD solar cell is illustrated in Figure 4. The thickness of the CsSn$_{0.5}$Ge$_{0.5}$I3 layer was varied from 0.6 to 1 μm, and the corresponding evolution patterns of key parameters were analyzed. Firstly, the short-circuit current density (Jsc) (Figure 4(a)) exhibited a notable increase as the CsSn$_{0.5}$Ge$_{0.5}$I3 layer thickness was increased from 0.6 to 1 μm. Jsc values rose from 38.37 mA/cm^2 to approximately 38.49 mA/cm^2. This indicates that the thicker CsSn$_{0.5}$Ge$_{0.5}$I3 layer allowed for more efficient absorption of incident photons, leading to a higher generation of electron-hole pairs within the solar cell. Secondly, the fill factor (FF) (Figure 4(c)) showed a rapid rise as the CsSn$_{0.5}$Ge$_{0.5}$I3 layer

thickness increased. The FF increased from 57.5% to approximately 58.5%. A higher FF suggests improved charge extraction and reduced losses within the solar cell, contributing to enhanced overall efficiency. On the other hand, the open-circuit voltage (Voc) (Figure 4(b)) demonstrated a decrease with increasing $CsSn_{0.5}Ge_{0.5}I3$ layer thickness. Voc decreased from 1.286 V to approximately 1.266 V when the thickness reached 0.6 μm. The decrease in Voc can be attributed to various factors, including charge recombination losses or changes in energy level alignment at the interfaces. In summary, the inclusion of the CsSnCI3 layer in the solar cell configuration (IGZO / $CsSn_{0.5}Ge_{0.5}I3$ / CsSnCI3 / CsSnCI3 / Cu_2O / Spiro-OMeTAD) resulted in increased light absorption, leading to a higher generation of electron-hole pairs. This improvement in the overall efficiency of the solar cell is attributed to the increased capture of photons and their conversion into electrical current.
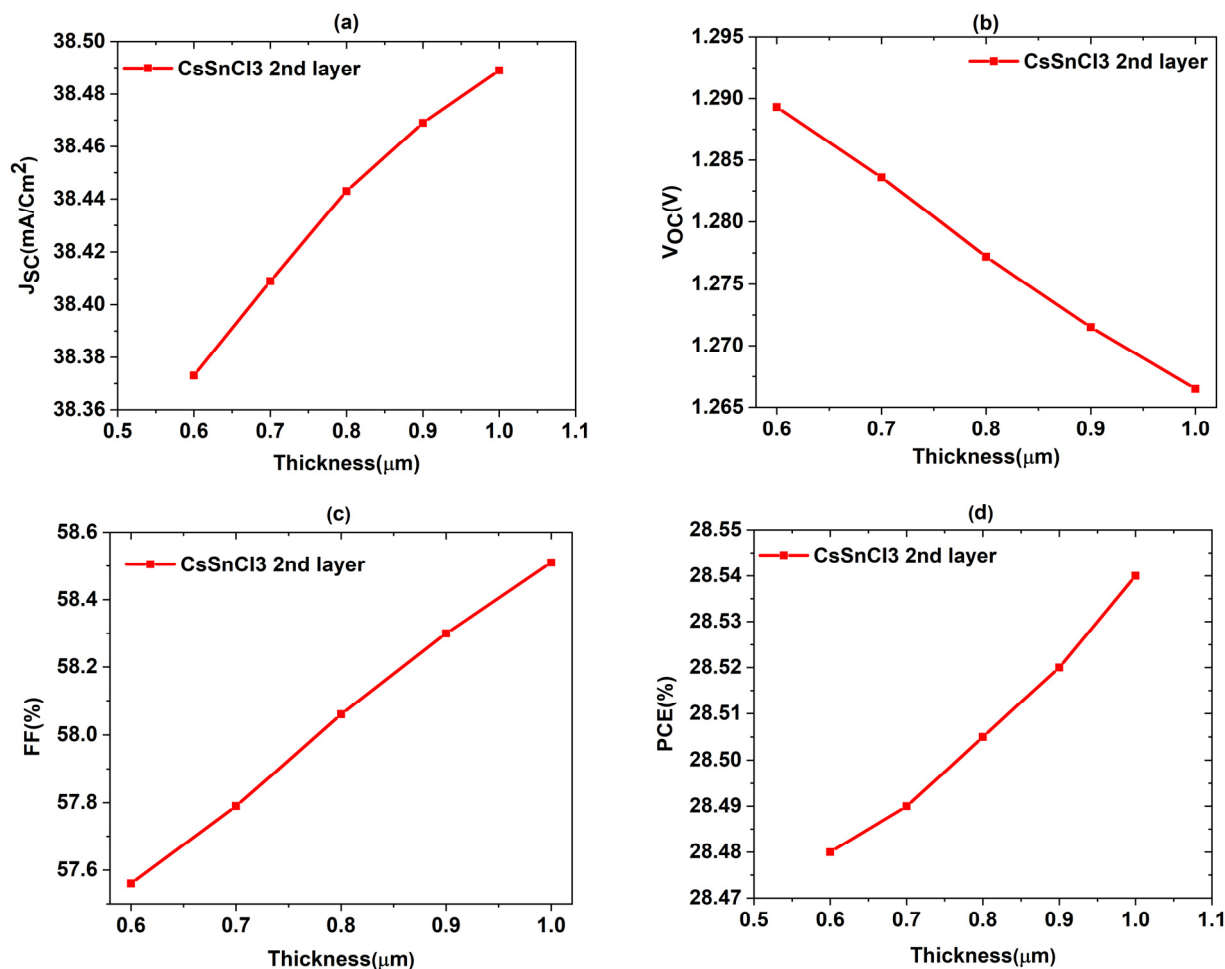
Fig. 4 – Effect of the second perovskite layer (CsSnCI3) thickness

3.3. Effect of the third perovskite layer (CsSnCI3) thickness:

The impact of the n-CsSnCI3 third absorber layer thickness on the performance of the IGZO/$CsSn_{0.5}Ge_{0.5}I3$/CsSnCI3/CsSnCI3/Cu_2O/Spiro-OMeTAD solar cell is depicted in Figure 5. The study involved varying the thickness of the $CsSn_{0.5}Ge_{0.5}I3$ layer from 1 to 1.5 μm, and the corresponding changes in key parameters were analyzed. Initially, the short-circuit current density (Jsc) (Figure 5(a)) displayed a noticeable decrease as the thickness of the $CsSn_{0.5}Ge_{0.5}I3$ third layer increased from 1 to 1.5 μm. The Jsc values decreased from 38.27 mA/cm² to approximately 38 mA/cm². This decrease in Jsc suggests that the thicker CsSnCI3 layer may have an impact on charge carrier generation. Non-uniform photon absorption throughout the thickness of the CsSnCI3 layer could lead to reduced effective generation of electron-hole pairs. This non-uniform absorption might arise from recombination losses or inefficient charge transport within the thicker layer, resulting in a decrease in Jsc. Conversely, the fill factor (FF) (Figure 5(c)) exhibited a rapid increase as the thickness of the $CsSn_{0.5}Ge_{0.5}I3$ third layer increased, the FF increased from 54.1% to approximately 55.4%. The increased thickness of the n-CsSnCI3 layer improved charge carrier collection and reduced charge carrier recombination, resulting in a higher fill factor. This enhancement is attributed to the thicker layer providing more pathways for charge carriers to reach the electrodes, minimizing losses and maximizing the overall power output. However, the open-circuit voltage (Voc) (Figure 5(b)) demonstrated a decrease with increasing $CsSn_{0.5}Ge_{0.5}I3$ layer thickness, Voc decreased from 1.382 V to approximately 1.346 V when the thickness reached 1.5 μm. The alteration of band alignment and energy levels, caused by the increased thickness

of the n-CsSnCI3 layer, contributed to this reduction in Voc. These changes in energy levels resulted in a reduced built-in potential, increased recombination, or modified charge carrier extraction, all of which contributed to the lower Voc observed. Moreover, the power conversion efficiency (PCE) (Figure 5(d)) also experienced a decrease with increasing $CsSn_{0.5}Ge_{0.5}I3$ layer thickness. Voc decreased from 28.64% to approximately 28.5% when the thickness reached 1.5 μm. The thicker n-CsSnCI3 layer introduced additional losses, such as increased resistive losses or reduced light absorption due to inefficient charge transport or light scattering. These losses further contributed to the overall decrease in the PCE of the solar cell.
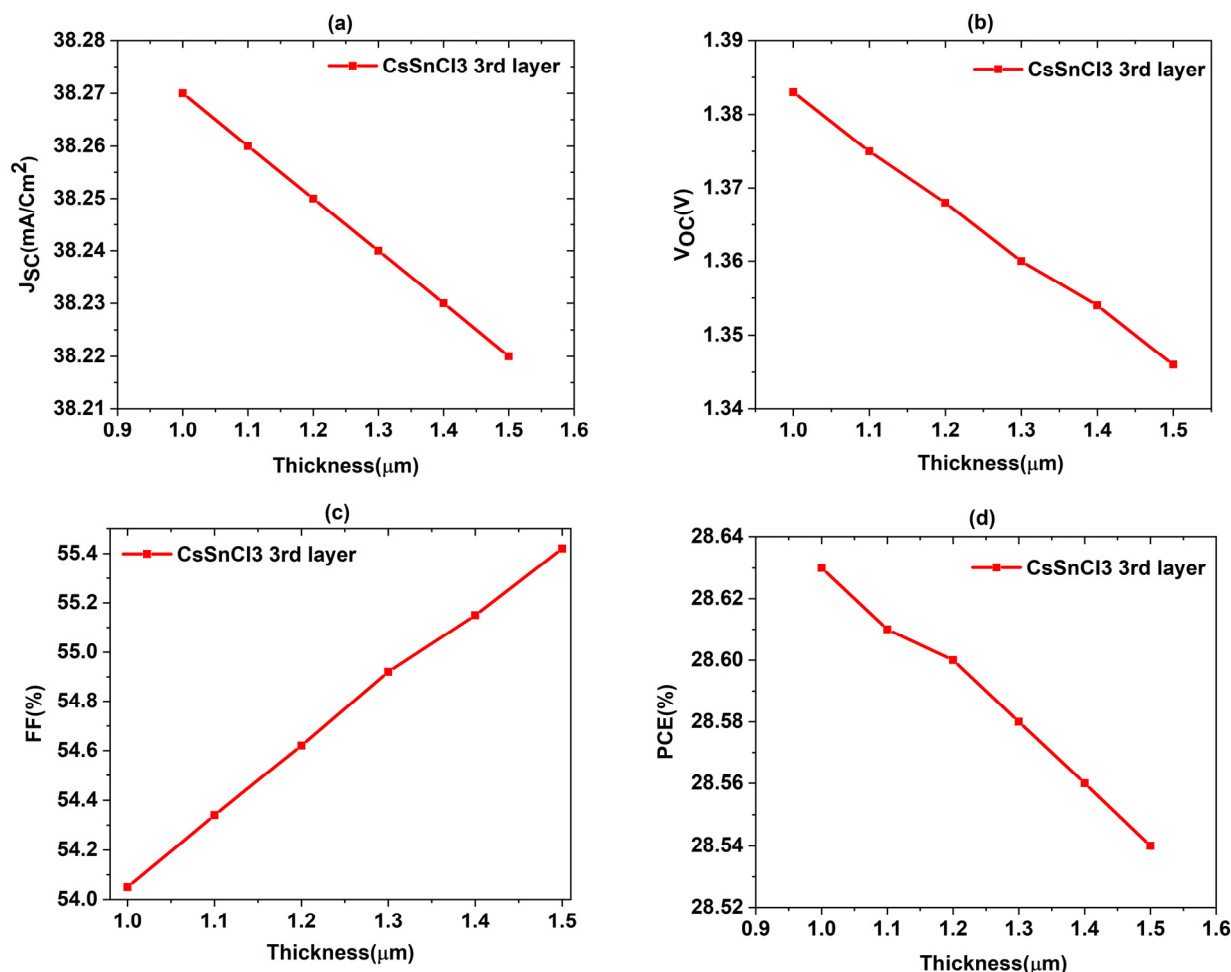
Figure 5. Effect of the third perovskite layer (CsSnCI3) thickness

3.4. Effect of the layer (ETL) thickness

In a perovskite solar cell, the Electron Transport Layer (ETL) plays a crucial role in enhancing the overall performance of the device by facilitating the movement of electrons from the perovskite layer to the front contact. In this study, we will examine the impact of varying ETL thickness on the output performance of the $IGZO/CsSn_{0.5}Ge_{0.5}I3/CsSnCI3/CsSnCI3/Cu_2O/Spiro-OMeTAD$ solar cell, as depicted in Figure 6. By analyzing the evolution of key parameters, we can understand how changes in ETL thickness affect the device's characteristics. Firstly, the short-circuit current density (Jsc) (Figure 6(a)) experiences a noticeable decrease as the ETL layer thickness increases from 0.02 to 0.17 μm. Specifically, Jsc values decrease from 38.40 mA/cm^2 to approximately 38.2 mA/cm^2. This decrease can be attributed to the phenomenon where a thicker ETL layer absorbs a greater amount of incident photons within the ETL itself. Consequently, a portion of the incident light is prevented from reaching the $CsSn_{0.5}Ge_{0.5}I3$ absorber layer, leading to a reduction in the generation of charge carriers through photon absorption. Secondly, the fill factor (FF) (Figure 6(c)) demonstrates a rapid decline with increasing ETL layer thickness. The FF decreases from 60.4% to approximately 59.7%. The introduction of the ETL layer introduces additional resistance within the solar cell. This increased resistance impedes the efficient extraction and transport of charges, resulting in higher losses and a decrease in FF. Furthermore, both the open-circuit voltage (Voc) (Figure 6(b)) and power conversion efficiency (PCE) (Figure 6(d)) exhibit a decrease as the ETL layer thickness increases. This reduction in Voc and PCE can be attributed to multiple factors. For instance, a thicker ETL layer can introduce increased series resistance within the device, hindering the efficient flow of current. Consequently, a voltage drop occurs across the ETL layer, leading to a reduction in Voc. In summary, the thickness of the ETL layer in a perovskite solar cell has a significant influence on its performance. While a thicker ETL layer enhances

photon absorption within itself, it simultaneously hampers the flow of charge carriers, resulting in decreased Jsc, FF, Voc, and PCE. These findings highlight the importance of carefully optimizing the ETL thickness to achieve optimal performance in perovskite solar cells.
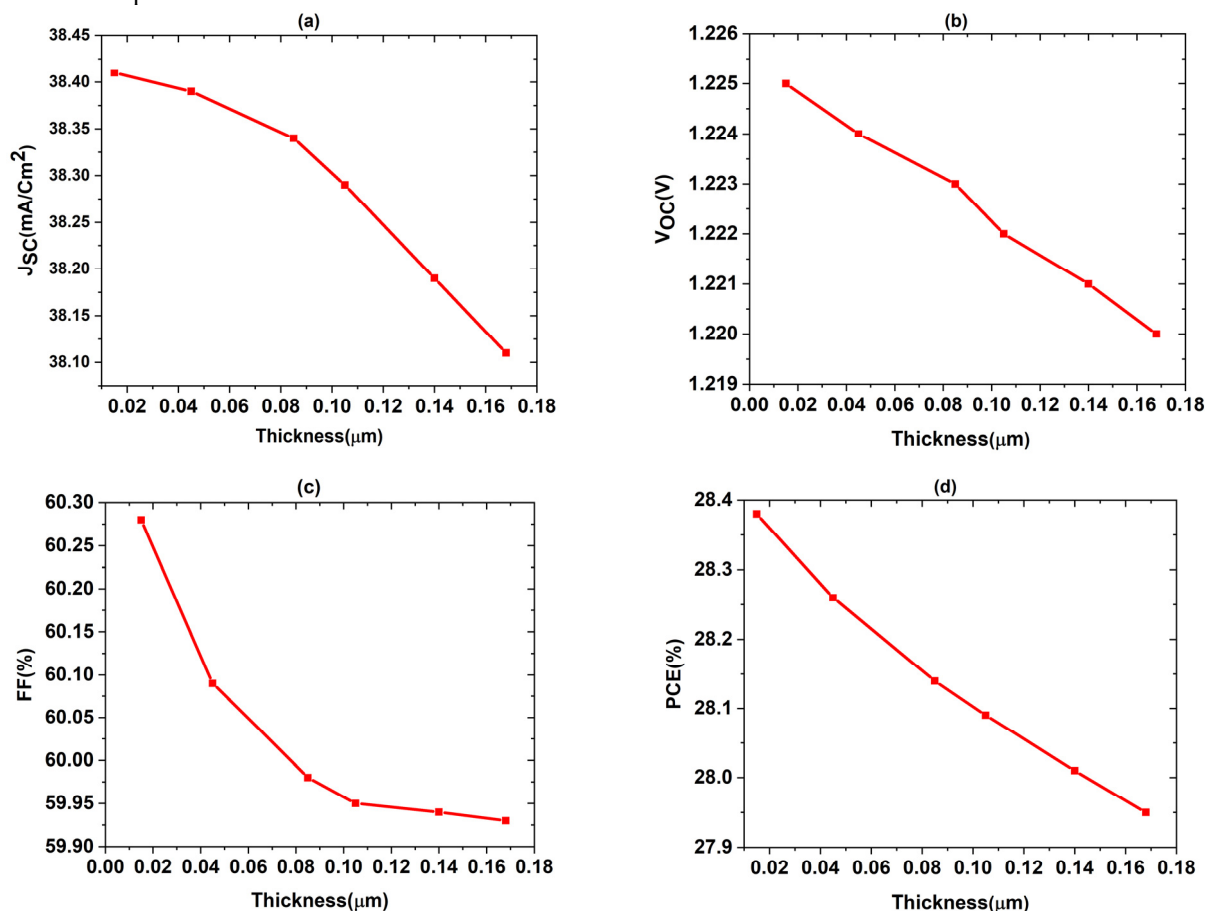
Figure 6. Effect of the layer (ETL) thickness

3.5. Effect of the layer (HTL) thickness

The influence of the hole transport layer (HTL) thickness on key performance parameters, including open-circuit voltage (Voc), short-circuit current density (Jsc), fill factor (FF), and overall efficiency, was investigated and depicted in Figure 7. Surprisingly, it was observed that varying the HTL thickness had negligible impact on these parameters. This phenomenon can be attributed to the high absorption of photons by the absorber and electron transport layers (ETL), resulting in the majority of available photons being absorbed before reaching the HTL layer. Consequently, only a small number of charge carriers are generated within the HTL layer, limiting its influence on the device performance. To further elucidate this behavior, the values of Voc and Jsc were examined, as depicted in Figure 7(a) and (b) respectively. It was found that Voc remained relatively constant at around 1.47V, while Jsc exhibited a consistent value of approximately 38.51 mA/cm^2. These observations indicate that the HTL thickness variation has minimal impact on these two parameters. Additionally, the fill factor (FF) and efficiency were evaluated and presented in Figure 7(c) and (d) respectively. Notably, both FF and efficiency demonstrated a stable behavior, hovering around 50% and 29% respectively, regardless of the HTL thickness. These findings suggest that, in this particular solar cell configuration, the HTL thickness does not significantly affect the device performance. The limited carrier generation within the HTL layer, due to the substantial photon absorption in previous layers, mitigates its role in determining Voc, Jsc, FF, and efficiency. It is important to note that these conclusions are specific to the investigated solar cell structure, and different device configurations may exhibit diverse responses to HTL thickness variations.

Table 2 presents the design structure that has been achieved through the optimization of layer thicknesses.

Table 2. Comparison between the conventional and the suggested model

Structure	J$_{SC}$ (mA/cm^2)	V$_{OC}$(V)	FF (%)	PCE (%)
FTO/ZnO/ CsSn0.5Ge0.5I3/CuI/Au [31]	24.21	1.203	84.07	24.51
FTO/IGZO/CsSn0.5Ge0.5I3/ CsSnCI3/ CsSnCI3/CuO2/Au	38.4	1.486	52.48	28.96

This table provides a comparison between the optimized designs and a non-optimized cell, specifically referred to as the reference cell [37]. The findings in Table 2 clearly demonstrate a significant improvement in performance for the optimized designs when compared to the non-optimized variant. The results obtained from our simulations indicate a

favorable alignment between the performance of the reference cell [37] and our optimized designs. This suggests that our simulation results closely resemble the outcomes reported in the reference study.
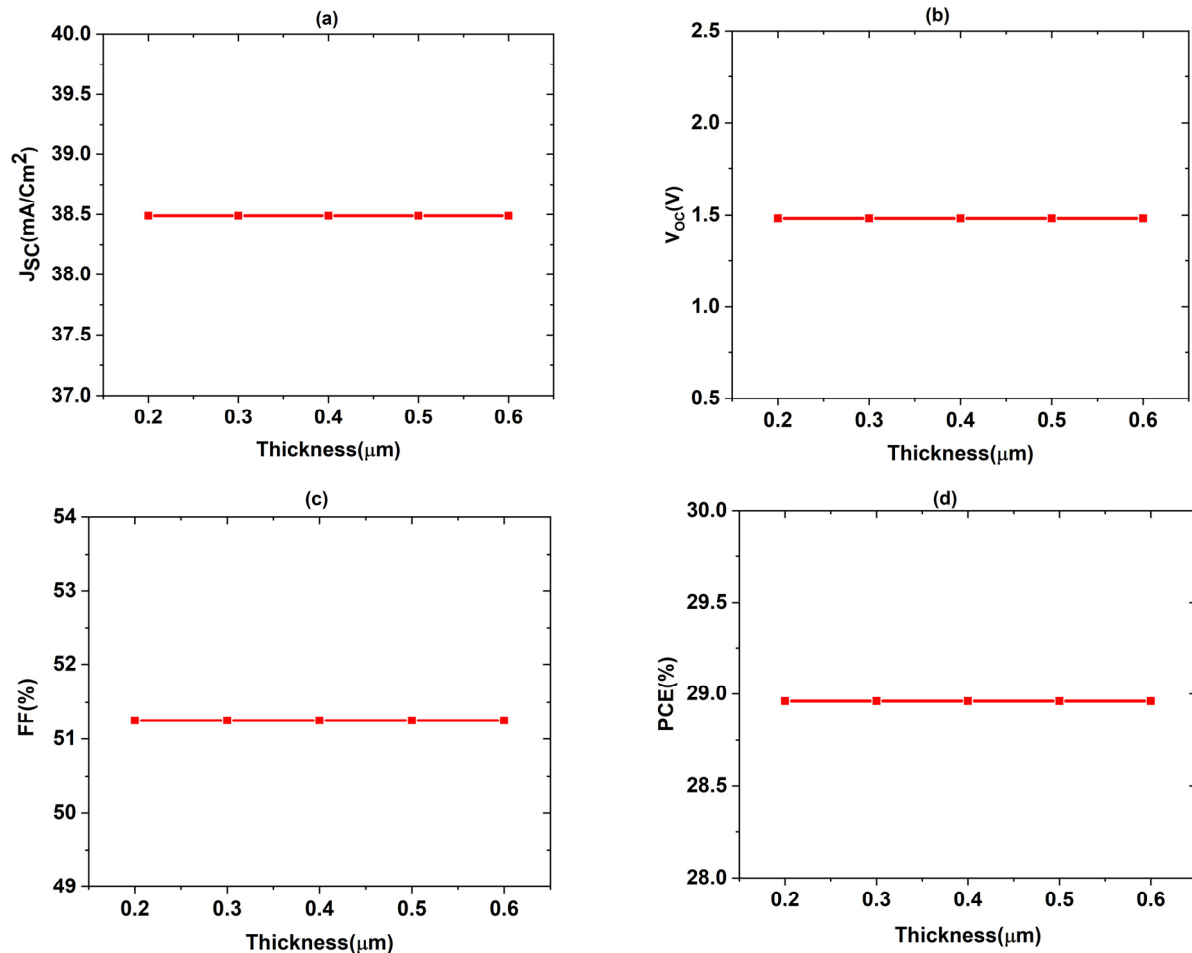
Figure 7. Effect of the layer (HTL) thickness

4. CONCLUSION

In summary, this study investigates the results of a comprehensive simulation study on the influence of a triple absorber layer configuration in a perovskite-based solar cell using the SCAPS-1D software, under AM1.5 illumination. The simulated structure comprises a Cesium Tin-Germanium Tri-iodide ($CsSn_{0.5}Ge_{0.5}I3$) absorber layer sandwiched between IGZO and Cu_2O layers. The main objective of this study is to enhance the power conversion efficiency (PCE) by optimizing the thicknesses of each layer. To validate our simulation results, we compare them with experimental data obtained from existing literature, and we observe a satisfactory agreement between the two. Our findings reveal that the maximum PCE of 28% can be achieved by utilizing specific thickness values for each layer. Specifically, the optimal thicknesses are determined to be 20 nm for the IGZO layer, 200 nm for the Cu_2O layer, and 700 nm for the perovskite layer. These optimized thickness values lead to a significant improvement in the PCE of the solar cell, reaching 29%. This achievement highlights the effectiveness of our proposed triple absorber layer configuration and demonstrates its potential to enhance the overall performance of the perovskite-based solar cell. Overall, this study provides valuable insights into the optimization of the absorber layer configuration in perovskite solar cells, leading to improved power conversion efficiency.

ORCID
Abderrahim Yousfi, https://orcid.org/0000-0003-2071-728X; Okba Saidani, https://orcid.org/0000-0003-0507-5581
Zitouni Messai, https://orcid.org/0000-0002-2508-3696

REFERENCES
[1] N.J. Jeon, H. Na, E.H. Jung, T.-Y. Yang, Y.G. Lee, G. Kim, H.-W. Shin, et al., "A fluorene-terminated hole-transporting material for highly efficient and stable perovskite solar cells," Nature Energy, **3**(8), 682-689 (2018). https://doi.org/10.1038/s41560-018-0200-6

[2] N. Li, Z. Zhu, J. Li, A.K.-Y. Jen, L. Wang, "Inorganic $CsPb_{1-x}Sn_xIBr_2$ for efficient wide-bandgap perovskite solar cells," Advanced energy materials, **8**(22), 1800525 (2018). https://doi.org/10.1002/aenm.201800525

[3] F. Zhang, B. Yang, Y. Li, W. Deng, and R. He, "Extra-long electron–hole diffusion lengths in $CH_3NH_3PbI_{3-x}Cl_x$ perovskite single crystals," Journal of Materials Chemistry C, **5**(33), 8431-8435 (2017). https://doi.org/10.1039/C7TC02802D

[4] Q. Ou, X. Bao, Y. Zhang, H. Shao, G. Xing, X. Li, L. Shao, et al., "Band structure engineering in metal halide perovskite nanostructures for optoelectronic applications," Nano Materials Science, **1**(4), 268-287 (2019). https://doi.org/10.1016/j.nanoms.2019.10.004

[5] K. Tanaka, T. Takahashi, T. Ban, T. Kondo, K. Uchida, and N. Miura, "Comparative study on the excitons in lead-halide-based perovskite-type crystals $CH_3NH_3PbBr_3$ $CH_3NH_3PbI_3$," Solid state communications, **127**(9-10), 619-623 (2003). https://doi.org/10.1016/S0038-1098(03)00566-0

[6] K. Yamada, H. Kawaguchi, T. Matsui, T. Okuda, and S. Ichiba, "Structural Phase Transition and Electrical Conductivity of the Perovskite $CH_3NH_3Sn_{1-x}Pb_xBr_3$ and $CsSnBr_3$," Bulletin of the Chemical Society of Japan, **63**(9), 2521-2525 (1990). https://doi.org/10.1246/bcsj.63.2521

[7] M.S. Chowdhury, S.A. Shahahmadi, P. Chelvanathan, S.K. Tiong, N. Amin, K. Techato, N. Nuthammachot, et al., "Effect of deep-level defect density of the absorber layer and n/i interface in perovskite solar cells by SCAPS-1D," Results in Physics, **16**, 102839 (2020). https://doi.org/10.1016/j.rinp.2019.102839

[8] M.A. Green, E.D. Dunlop, J. Hohl-Ebinger, M. Yoshita, N. Kopidakis, and X. Hao, "Solar cell efficiency tables (Version 58)," Progress in photovoltaics: research and applications, **29**(7), 657-667 (2021). https://doi.org/10.1002/pip.3506

[9] Y. Jiang, E.J. Juarez-Perez, Q. Ge, S. Wang, M.R. Leyden, L.K. Ono, S.R. Raga, et al., "Post-annealing of MAPbI 3 perovskite films with methylamine for efficient perovskite solar cells," Materials Horizons, **3**(6), 548-555 (2016). https://doi.org/10.1039/C6MH00160B

[10] Y.H. Khattak, F. Baig, A. Shuja, S. Beg, and B.M. Soucase, "Numerical analysis guidelines for the design of efficient novel nip structures for perovskite solar cell," Solar Energy, **207**, 579-591 (2020). https://doi.org/10.1016/j.solener.2020.07.012

[11] A. Kojima, K. Teshima, Y. Shirai, and T. Miyasaka, "Organometal halide perovskites as visible-light sensitizers for photovoltaic cells," Journal of the American Chemical Society, **131**(17), 6050-6051 (2009). https://doi.org/10.1021/ja809598r

[12] J. Wu, Y. Li, Y. Li, W. Xie, J. Shi, D. Li, S. Cheng, and Q. Meng, "Using hysteresis to predict the charge recombination properties of perovskite solar cells," Journal of Materials Chemistry A, **9**(10), 6382-6392 (2021). https://doi.org/10.1039/D0TA12046D

[13] J.J. Yoo, G. Seo, M.R. Chua, T.G. Park, Y. Lu, F. Rotermund, Y.-K. Kim, et al., "Efficient perovskite solar cells via improved carrier management," Nature, **590**(7847), 587-593 (2021). https://doi.org/10.1038/s41586-021-03285-w

[14] H. Min, D.Y. Lee, J. Kim, G. Kim, K.S. Lee, J. Kim, M.J. Paik, et al., "Perovskite solar cells with atomically coherent interlayers on SnO_2 electrodes," Nature, **598**(7881), 444-450 (2021). https://doi.org/10.1038/s41586-021-03964-8

[15] T. Krishnamoorthy, H. Ding, C. Yan, W.L. Leong, T. Baikie, Z. Zhang, M. Sherburne, et al., "Lead-free germanium iodide perovskite materials for photovoltaic applications," Journal of Materials Chemistry A, **3**(47), 23829-23832 (2015). https://doi.org/10.1039/C5TA05741H

[16] M.H. Kumar, S. Dharani, W.L. Leong, P.P. Boix, R.R. Prabhakar, T. Baikie, C. Shi, et al., "Lead-free halide perovskite solar cells with high photocurrents realized through vacancy modulation," Advanced Materials, **26**(41), 7122-7127 (2014). https://doi.org/10.1002/adma.201401991

[17] B. Wu, Y. Zhou, G. Xing, Q. Xu, H.F. Garces, A. Solanki, T.W. Goh, et al., "Long minority-carrier diffusion length and low surface-recombination velocity in inorganic lead-free CsSnI3 perovskite crystal for solar cells," Advanced Functional Materials, **27**(7), 1604818 (2017). https://doi.org/10.1002%2Fadfm.201604818

[18] H. Wei, P. Qiu, Y. Li, Y. He, M. Peng, X. Zheng, and X. Liu, "Challenges and strategies of all-inorganic lead-free halide perovskite solar cells," Ceramics International, **48**(5), 5876-5891 (2022). https://doi.org/10.1016/j.ceramint.2021.11.184

[19] M.-G. Ju, M. Chen, Y. Zhou, J. Dai, L. Ma, N.P. Padture, and X.C. Zeng, "Toward eco-friendly and stable perovskite materials for photovoltaics," Joule, **2**(7), 1231-1241 (2018). https://doi.org/10.1016/j.joule.2018.04.026

[20] T. Leijtens, G.E. Eperon, N.K. Noel, S.N. Habisreutinger, A. Petrozza, and H.J. Snaith, "Stability of metal halide perovskite solar cells," Adv. Energy Mater, **5**, 1500963 (2015). https://doi.org/10.1002/aenm.201500963

[21] M. Chen, M.-G. Ju, H.F. Garces, A.D. Carl, L.K. Ono, Z. Hawash, Y. Zhang, et al., "Highly stable and efficient all-inorganic lead-free perovskite solar cells with native-oxide passivation," Nature communications, **10**(1), 16 (2019). https://doi.org/10.1038/s41467-018-07951-y

[22] G.G. Chan, C.M. Koch, and L.H. Connors, "Blood proteomic profiling in inherited (ATTRm) and acquired (ATTRwt) forms of transthyretin-associated cardiac amyloidosis," Journal of Proteome Research, **16**(4), 1659-1668 (2017). https://doi.org/10.1021/acs.jproteome.6b00998

[23] E.L. Unger, L. Kegelmann, K. Suchan, D. Sörell, L. Kortec, and S. Albrecht, "Roadmap and roadblocks for the band gap tunability of metal halide perovskites," Journal of Materials Chemistry A, **5**(23), 11401-11409 (2017). https://doi.org/10.1039/C7TA00404D

[24] M. Saliba, T. Matsui, J.-Y. Seo, K. Domanski, J.-P. Correa-Baena, M.K. Nazeeruddin, S.M. Zakeeruddin, et al., "Cesium-containing triple cation perovskite solar cells: improved stability, reproducibility and high efficiency," Energy & environmental science, **9**(6), 1989-1997 (2016). https://doi.org/10.1039/C5EE03874J

[25] P. Roy, and A. Khare, "Analysis of an efficient and eco-friendly CsGeSnI3 based perovskite solar cell: A theoretical study," Materials Today: Proceedings, **44**, 2997-3000 (2021). https://doi.org/10.1016/j.matpr.2021.02.253

[26] T. Kamiya, K. Nomura, and H. Hosono, "Present status of amorphous In–Ga–Zn–O thin-film transistors," Science and Technology of Advanced Materials, (2010). https://doi.org/10.1088/1468-6996/11/4/044305

[27] H. Hosono, J. Kim, Y, Toda, and S. Watanabe, "Transparent amorphous oxide semiconductors for organic electronics: Application to inverted OLEDs," Proceedings of the National Academy of Sciences, **114**(2), 233-238 (2017). https://doi.org/10.1073/pnas.1617186114

[28] T. Minami, Y. Nishi, T. Miyata, and J.-I. Nomoto, "High-efficiency oxide solar cells with ZnO/Cu_2O heterojunction fabricated on thermally oxidized Cu_2O sheets," Applied physics express, **4**(6), 062301 (2011). https://doi.org/10.1143/APEX.4.062301

[29] N.K. Singh, and A. Agarwal, "Performance assessment of sustainable highly efficient CsSn0. 5Ge0. 5I3/FASnI3 based Perovskite Solar Cell: A numerical modelling approach," Optical Materials, **139**, 113822 (2023). https://doi.org/10.1016/j.optmat.2023.113822

[30] S. Bhatt, R. Shukla, C. Pathak, and S. K. Pandey, "Evaluation of performance constraints and structural optimization of a core-shell ZnO nanorod based eco-friendly perovskite solar cell," Solar Energy, **215**, 473-481 (2021). https://doi.org/10.1016/j.solener.2020.12.069

[31] Raghvendra, R.R. Kumar, and S.K. Pandey, "Performance evaluation and material parameter perspective of eco-friendly highly efficient CsSnGeI3 perovskite solar cell," Superlattices and Microstructures, **135**, 106273 (2019). https://doi.org/10.1016/j.spmi.2019.106273

[32] M. Burgelman, P. Nollet, and S. Degrave, "Modelling polycrystalline semiconductor solar cells," Thin Solid Films, **361-362**, 527–532 (2000). https://doi.org/10.1016/S0040-6090(99)00825-1

[33] N.K. Singh, A. Agarwal, T. Kanumuri, and T. Varshney, "A Study of an Inorganic-Organic HTM on the Implementation of Lead based PSC Device," in: *2020 IEEE Students Conference on Engineering & Systems (SCES)*, (IEEE, 2020). pp. 1-6. https://doi.org/10.1109/SCES50439.2020.9236734

[34] N. Nikfar, and N. Memarian, "Theoretical study on the effect of electron transport layer parameters on the functionality of double-cation perovskite solar cells," Optik, **258**, 168932 (2022). https://doi.org/10.1016/j.ijleo.2022.168932

[35] Y.T. Li, C.F. Han, and J.F. Lin, "Characterization of the electrical and optical properties for a-IGZO/Ag/a-IGZO triple-layer thin films with different thickness depositions on a curved glass substrate," Optical Materials Express, **9**(8), 3414-3431 (2019). https://doi.org/10.1364/OME.9.003414

[36] V.K. Jayaraman, A.M. Álvarez, and M. de la luz O. Amador, "Effect of substrate temperature on structural, morphological, optical and electrical properties of IGZO thin films," Physica E: Low-dimensional Systems and Nanostructures, **86**, 164-167 (2017). https://doi.org/10.1016/j.physe.2016.10.029

[37] S. Bouazizi, W. Tlili, A. Bouich, B.M. Soucase, and A. Omri, "Design and efficiency enhancement of FTO/PC60BM/CsSn0. 5Ge0. 5I3/Spiro-OMeTAD/Au perovskite solar cell utilizing SCAPS-1D Simulator," Materials Research Express, **9**(9), 096402 (2022). https://doi.org/10.1088/2053-1591/ac8d52

[38] F. Azri, A. Meftah, N. Sengouga, and A. Meftah, "Electron and hole transport layers optimization by numerical simulation of a perovskite solar cell," Solar energy, **181**, 372-378 (2019). https://doi.org/10.1016/j.solener.2019.02.017

[39] M. Jamil, A. Ali, K. Mahmood, M.I. Arshad, S. Tahir, M.A. Nabi, S. Ikram, N. Amin, and S. Hussain, "Numerical simulation of perovskite/Cu2Zn (Sn1-xGex)S4 interface to enhance the efficiency by valence band offset engineering," Journal of Alloys and Compounds, **821**, 153221 (2020). https://doi.org/10.1016/j.jallcom.2019.153221

ПРОЕКТУВАННЯ ТА МОДЕЛЮВАННЯ ПЕРОВСКІТНОГО СОНЯЧНОГО ЕЛЕМЕНТА З ПОТРІЙНИМ ПОГЛИНАЮЧИМ ШАРОМ ДЛЯ ВИСОКОЇ ЕФЕКТИВНОСТІ ПЕРЕТВОРЕННЯ

Абдеррахім Юсфі[a], Окба Сайдані[a], Зітуні Мессаі[a], Рафік Зуахе[b]
Мохамед Меддах[a], Юнес Белгумрі[a]
[a] Лабораторія ETA, кафедра електроніки, технологічний факультет, Університет Мохамеда Ель Бачіра Ель Ібрагімі Бордж Бу Аррерідж-34030, Алжир
[b] Кафедра електроніки, технологічний факультет, Університет Мсіла, 28000, Алжир

У цьому документі представлено комплексне моделювання впливу конфігурації потрійного поглинаючого шару в сонячному елементі на основі перовскіту з використанням програмного забезпечення SCAPS-1D під освітленням AM1.5. Змодельована структура містить шар поглинача із цезію, олова та трийодиду германію ($CsSn_{0,5}Ge_{0,5}I_3$), розміщеного між шарами оксиду індію, галію, цинку (IGZO) та Cu_2O. Основною метою цього дослідження є підвищення ефективності перетворення електроенергії (PCE) шляхом оптимізації товщини кожного шару. Щоб перевірити наші результати моделювання, ми порівнюємо їх з експериментальними даними, отриманими з існуючої літератури, і спостерігаємо задовільну згоду між ними. Наші висновки показують, що максимального PCE 28% можна досягти, використовуючи конкретні значення товщини для кожного шару. Зокрема, визначено оптимальну товщину 20 нм для шару IGZO, 200 нм для шару Cu_2O та 700 нм для шару перовскіту. Ці оптимізовані значення товщини призводять до значного покращення PCE сонячної батареї, досягаючи 29%. Це досягнення підкреслює ефективність запропонованої нами конфігурації потрійного поглинаючого шару та демонструє її потенціал для підвищення загальної продуктивності сонячної батареї на основі перовскіту. Загалом це дослідження дає цінну інформацію щодо оптимізації конфігурації шару поглинача в перовскітних сонячних елементах, що призводить до підвищення ефективності перетворення електроенергії.
Ключові слова: *перовскітний сонячний елемент; $CsSn_{0,5}Ge_{0,5}I_3$; ефективність перетворення потужності; SCAPS-1D*